Recent Res. Devel. Microwave Theory & Tech., 1 (1999): 25-35

Analysis of waveguide discontinuities by the coupled-integral-equations technique

Jens Bornemann[1], Smain Amari[2] and Rüdiger Vahldieck[2]
[1]Department of Electrical and Computer Engineering, University of Victoria, Box 3055, Victoria, BC Canada V8W 3P6
[2]Laboratory for Electromagnetic Fields and Microwave Electronics, Swiss Federal Institute of Technology, Gloriastr. 35 CH-8092 Zürich, Switzerland

ABSTRACT

The coupled-integral-equations technique (CIET) as applied to arbitrary waveguide discontinuities is presented. This makes the CIET applicable to general optimization algorithms which may alter the nature of discontinuities during the optimization process. The general procedure of arriving at coupled integral equations is highlighted, and the computational effort involving the final matrix equation is discussed. Several analysis and design examples involving simple discontinuities and entire waveguide components demonstrate the efficiency and versatility of the CIET. Applications in coordinate systems other than the cartesian demonstrate the method's flexibility. All examples are confirmed by results obtained from the mode-matching technique (MMT) or by a commercial field solver. CPU-time ratios between the CIET and MMT demonstrate the advantages of the CIET. Particularly in narrowband systems, this ratio increases tremendously in favour of the CIET.

I. INTRODUCTION

Waveguide discontinuities and components have been traditionally analyzed by using the mode-matching technique (MMT) [1], [2]. For many applications, MMT offers a reasonably fast design procedure which allows for optimization routines to be incorporated [1]. If boundary conditions do not fall in line with the unit vectors of the respective coordinate system, however, MMT requires staircase approximations for the geometries which usually puts it at a disadvantage compared to more generally oriented field solvers, e.g., [3]. In some cases, a combination of both, e.g. [4], has been shown to alleviate some of the problems.

All of these methods consume substantial computing resourses when narrowband systems are to be analyzed. This is due to extremely fine mesh requirements in field solvers and an increasing number of modes in the MMT to obtain convergence of the scattering parameters. Not only in narrowband systems, but in general, the relatively slow convergence of the MMT and the phenomenon of relative convergence [2] have been linked to the inappropriate modelling of field singularities at metallic edges. This has been demonstrated in, e.g., [5], [6] where the effects of sharp metallic edges are taken into account in modified versions of the MMT. However, the interactions between multiple discontinuities is still determined by cascading the individual generalized scattering matrices, thereby considerably limiting the effects of the edge conditions.

Only if all edge conditions are simultaneously taken into account, i.e., if the interactions between closely spaced field singularities are adequately considered, then an accurate, reliable and fast procedure is obtained which has recently been introduced as the coupled-integral-equations technique (CIET) [7]. Besides retaining the salient features of the MMT, the CIET contains the influence of modes exclusively in the sums of matrix

element and not, as in the MMT, as separate matrix entries. Therefore, a much smaller matrix system with certain distinct properties, some of which will be discussed in this paper, is obtained.

The advantages of the CIET over the MMT have emerged as a result of more precisely specifying the structure under analysis by using a-priori information about the edge conditions at the discontinuities involved, e.g. [7]. This seems appropriate for the pure analysis of components and for the design of structures with predefined geometries such as, e.g., corrugations or irises. In a general optimization scenario, however, the geometry might be varied considerably, depending on the choices of goal (error) function and optimization procedure. For instance, an optimization routine might change an iris to a corrugation if such a measure helps improving the performance of the circuit.

Therefore, this paper focuses on making the CIET adaptable to such requests. An algorithm for general discontinuities formed by offset-connected waveguides is developed within the framework of the CIET. The formulation is demonstrated for rectangular waveguide discontinuities and components but may straightforwardly be converted to other coordinate systems, even mixed ones, as some of the examples will show. The algorithm is readily applicable to any two-port optimization procedure for waveguide technology and, based on the properties of the CIET, can easily be interfaced with multiport waveguide junctions for the design of entire waveguide systems.

II. THEORY

a) Single Discontinuity

For the derivation of the basic steps of this approach, we first consider the rectangular waveguide discontinuity depicted in Fig. 1. In this example, an incoming waveguide of cross-section $a_1 x b_1$ (region I) is connected to a waveguide of cross-section $a_2 x b_2$ (region II), and they share the common aperture area $a_0 x b_0$ (region 0). We will later consider individual cases in which the aperture area equals that of one of the two connected waveguides.

According to [1], the potential functions in the two waveguides i=I, II can be written as

$$T^{i}_{h(m,n)\to q} = \frac{2}{k^{i}_{cq}\sqrt{a_i b_i}} \cos\left\{\frac{m\pi}{a_i}(x-e_i)\right\}\cos\left\{\frac{n\pi}{b_i}(y-c_i)\right\} \frac{1}{\sqrt{1+\delta_{0m}}}\frac{1}{\sqrt{1+\delta_{0n}}} \quad (1)$$

$$T^{i}_{e(m,n)\to p} = \frac{2}{k^{i}_{cp}\sqrt{a_i b_i}} \sin\left\{\frac{m\pi}{a_i}(x-e_i)\right\}\sin\left\{\frac{n\pi}{b_i}(y-c_i)\right\} \quad (2)$$

where δ_{0k} is the Kronecker delta, and k_c denotes the cut-off wavelength. Note in Fig. 1 that the origin is taken to be the lower right corner of the incoming waveguide and, therefore, $e_1=c_1=0$. From (1) and (2), the transverse

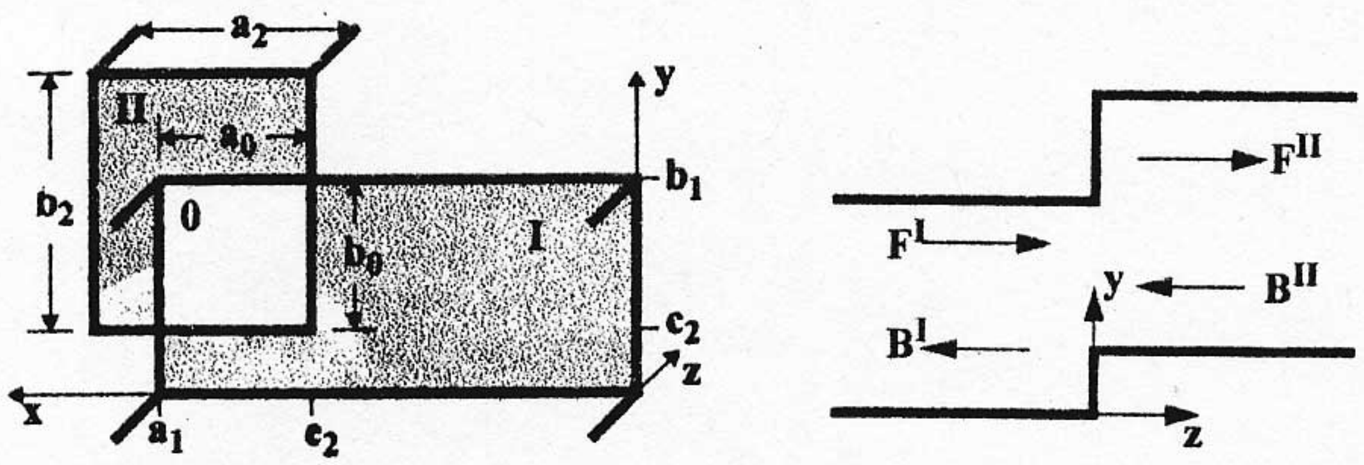

Figure 1: Arbitrary discontinuity formed by the connections of two waveguides; cross-sectional view (left) and sideview introducing wave amplitudes (right).

electromagnetic field is derived as

$$\vec{E}_T^i = \sum_q (\nabla T_{hq}^i \times \vec{e}_z) \cdot \left[F_{hq}^i \exp\left\{-jk_{zh_q}^i z\right\} + B_{hq}^i \exp\left\{jk_{zh_q}^i z\right\} \right] + \sum_p (-\nabla T_{ep}^i) \cdot \left[F_{ep}^i \exp\left\{-jk_{ze_p}^i z\right\} + B_{ep}^i \exp\left\{jk_{ze_p}^i z\right\} \right] \quad (3)$$

$$\vec{H}_T^i = \sum_q Y_{hq}^i (\nabla T_{hq}^i) \cdot \left[F_{hq}^i \exp\left\{-jk_{zh_q}^i z\right\} - B_{hq}^i \exp\left\{jk_{zh_q}^i z\right\} \right] + \sum_p Y_{ep}^i (\nabla T_{ep}^i \times \vec{e}_z) \cdot \left[F_{ep}^i \exp\left\{-jk_{ze_p}^i z\right\} - B_{ep}^i \exp\left\{jk_{ze_p}^i z\right\} \right] \quad (4)$$

where $Y_{h,e}$ are the admittances, $k_{zh,e}$ are the phase constants, and F and B are the amplitudes of the forward and backward traveling waves, respectively (Fig. 1).

The transverse electric fields at the discontinuity (z=0) are matched by introducing a vector function $\vec{X}(x, y)$ which is assumed to vanish everywhere except in the aperture plane. Thus we get

$$\vec{E}_T^I(x, y) = \vec{E}_T^{II}(x, y) = \vec{X}(x, y) \quad (5)$$

By using (3), (5) and multiplying with the orthogonal mode functions of regions I and II, the wave amplitude components in both regions i=I, II are isolated.

$$F_{hq}^i \exp\left\{-jk_{zh_q}^i z\right\} + B_{hq}^i \exp\left\{jk_{zh_q}^i z\right\} = \int_{y_l}^{y_u}\int_{x_l}^{x_u} (\nabla T_{hq}^i \times \vec{e}_z) \bullet \vec{X}(x, y)\,dx\,dy \quad (6)$$

$$F_{ep}^i \exp\left\{-jk_{ze_p}^i z\right\} + B_{ep}^i \exp\left\{jk_{ze_p}^i z\right\} = \int_{y_l}^{y_u}\int_{x_l}^{x_u} (-\nabla T_{ep}^i) \bullet \vec{X}(x, y)\,dx\,dy \quad (7)$$

The integration extends over the common aperture area, e.g., in the case of Fig. 1, $x_l=e_2$, $x_u=a_1$, $y_l=c_2$ and $y_u=b_1$. The vector function $\vec{X}(x, y)$ is chosen to contain the modal functions of the common aperture and the edge conditions at the metallic edges [8]. For the example in Fig. 1, we get

$$\vec{X}(x, y) = \sum_r \frac{[\nabla T_{hr}^0 \times \vec{e}_z] c_r}{[(x-x_u)(x_o-x)(y-y_u)(y_o-y)]^{1/3}} + \sum_s \frac{[-\nabla T_{es}^0] c_s}{[(x-x_u)(x_o-x)(y-y_u)(y_o-y)]^{1/3}} \quad (8)$$

where

$$T_{h(m,n)\to r}^0 = \cos\left\{\frac{m\pi}{a_0}(x-x_l)\right\}\cos\left\{\frac{n\pi}{b_0}(y-y_l)\right\} \quad (9)$$

$$T_{e(m,n)\to s}^0 = \sin\left\{\frac{m\pi}{a_0}(x-x_l)\right\}\sin\left\{\frac{n\pi}{b_0}(y-y_l)\right\} \quad (10)$$

By substituting (8) - (10) into (6) and (7) and solving the integrals for combinations (q,r), (q,s), (p,r) and (p,s), two coupling matrices similar to those in the mode-matching technique [1] are obtained

$$\left[\underline{W}^I\right] = \begin{bmatrix} \underline{W}_{hh}^I & \underline{W}_{he}^I \\ \underline{W}_{eh}^I & \underline{W}_{ee}^I \end{bmatrix}, \qquad \left[\underline{W}^{II}\right] = \begin{bmatrix} \underline{W}_{hh}^{II} & \underline{W}_{he}^{II} \\ \underline{W}_{eh}^{II} & \underline{W}_{ee}^{II} \end{bmatrix} \quad (11)$$

which represent the couplings from waveguide I and II to the common aperture area (region 0). Note first that submatrices $[\underline{W}_{he}]$ do not vanish - as they would in the MMT [1] - on account of the edge conditions in the vector basis functions; secondly, the entries of matrices $[\underline{W}]$ are frequency independent and need to be computed only once; thirdly, the mode spectrum is entirely determined by (1), (2), (9) and (10) and, therefore, field symmetries and reduced-mode sets can be considered in the same way as in the MMT.

Depending on the individual discontinuity, which might differ from that in Fig. 1, the positions of the edge conditions are decided on an individual basis. Fig. 2 shows several examples of discontinuitites in x-direction, and similar deliberations hold in y-direction. A straight connection of two identical waveguides (Fig. 2a), of course, does not require any edge conditions as there are no field singularities to be considered. If a dis-

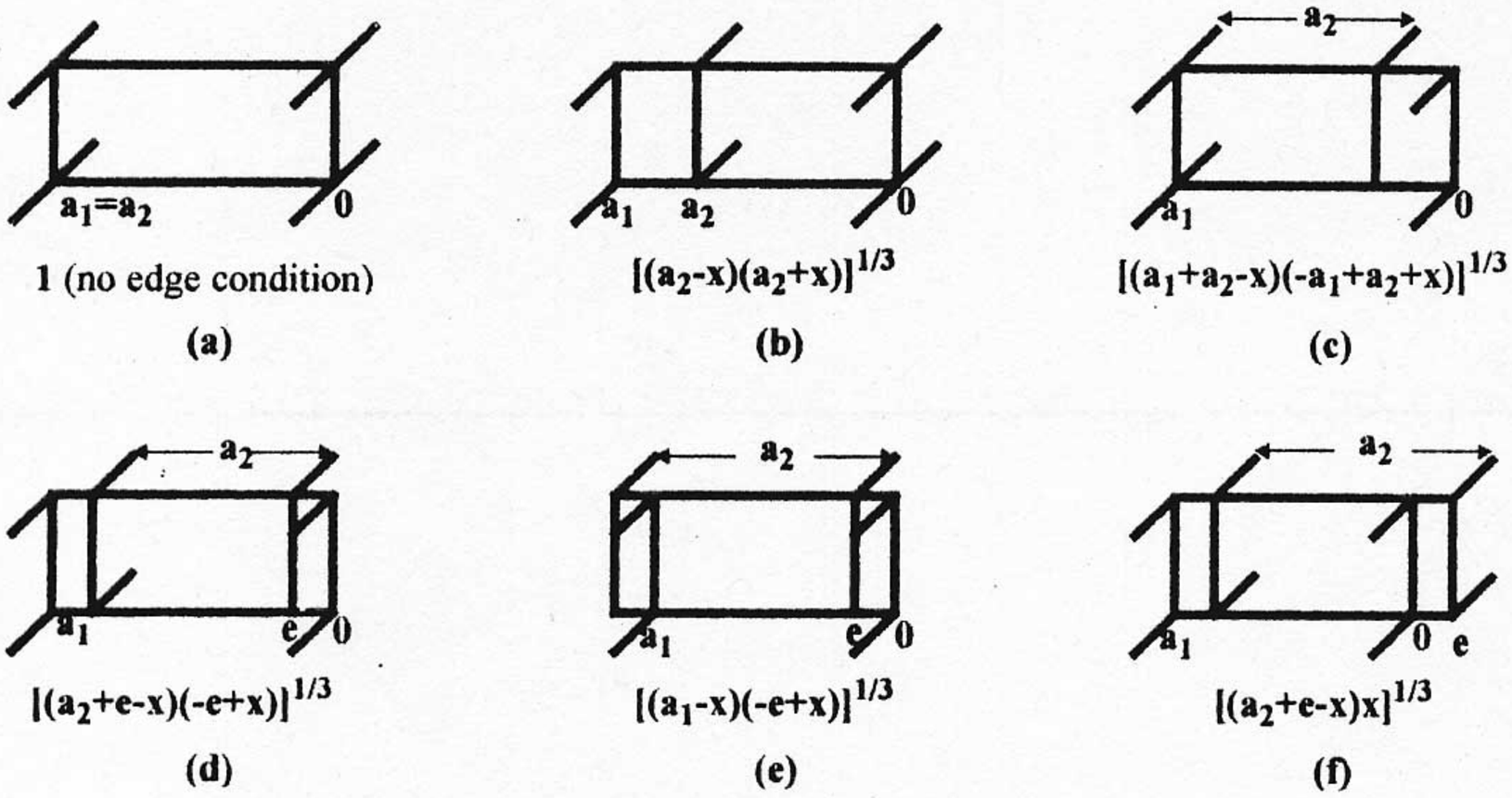

Figure 2: Denominator of the x-dependence of vector basis function in (8) for several discontinuities. Analogous considerations hold for the y-dependence.

continuity occurs at only one of the two walls (Fig. 2b, c), then the respective image is also taken into account. Two edge conditions at the boundaries of the aperture plane are required in all other cases (Fig. 2d, e, f), one of which (Fig. 2e) has been used in both directions in the example of Fig. 1.

Note that all integrals in (6) and (7) can be solved analytically by employing the following relationships [9].

$$\int_{-1}^{1} \frac{\cos(az)}{[1-z^2]^{1/3}}\,dz = \Gamma(1/2)\Gamma(2/3)\frac{J_{1/6}(|a|)}{[|a|/2]^{1/6}} \quad (12)$$

$$\int_{-1}^{1} \frac{dz}{[1-z^2]^{1/3}} = \frac{\Gamma(1/2)\Gamma(2/3)}{\Gamma(7/6)} \quad (13)$$

Routines for Bessel functions of fractional order are readily available, e.g., in [10].

b) *Multiple Discontinuities*

Matching the transverse magnetic fields (4) across the common aperture of Fig. 1 would result in an integral equation for the expansion coefficients c (c.f. (8)) from which the generalized scattering matrix of the discontinuity could be obtained, e.g. [5], [6]. However, this would lead to a modal combination of cascaded discontinuities as in the MMT, e.g. [1]. The powerful advantage of the coupled-integral-equations technique lies in the fact that all edge conditions at all discontinuities are taken into account *simultaneously*.

In order to accomplish this, we first combine TE- and TM-mode components and rewrite (6) and (7) for an arbitrary discontinuity i combining waveguide sections i-1 and i (Fig. 3)

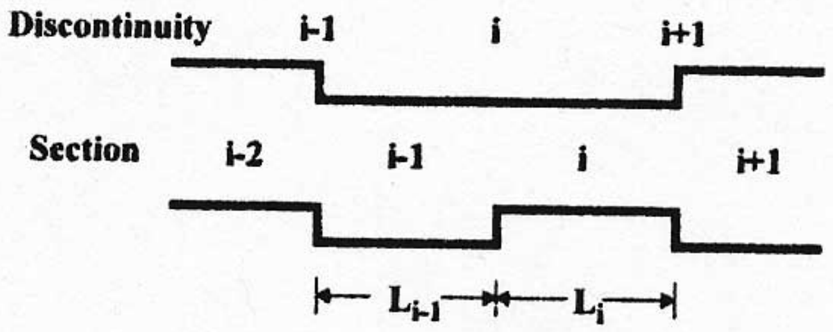

Figure 3: Discontinuity i and its neighbors in a multi-discontinuity environment.

$$F_k^{i-1}\exp\left\{-jk_{z_k}^{i-1}z\right\}+B_k^{i-1}\exp\left\{jk_{z_k}^{i-1}z\right\}=\sum_b W_{kb}^{I,i}c_b^i \tag{14}$$

$$F_k^i\exp\left\{-jk_{z_k}^i z\right\}+B_k^i\exp\left\{jk_{z_k}^i z\right\}=\sum_b W_{kb}^{II,i}c_b^i \tag{15}$$

and solve for the following terms needed in the matching conditions for the magnetic fields.

$$F_k^i-B_k^i=\sum_b\frac{-jW_{kb}^{II,i}c_b^i}{\tan\left\{k_{z_k}^i L_i\right\}}-\sum_b\frac{jW_{kb}^{I,i+1}c_b^{i+1}}{\sin\left\{k_{z_k}^i L_i\right\}} \tag{16}$$

$$F_k^{i-1}-B_k^{i-1}=\sum_b\frac{jW_{kb}^{I,i}c_b^i}{\tan\left\{k_{z_k}^{i-1}L_{i-1}\right\}}-\sum_b\frac{jW_{kb}^{II,i-1}c_b^{i-1}}{\sin\left\{k_{z_k}^{i-1}L_{i-1}\right\}} \tag{17}$$

Indices k and b denote a mode and a basis function, respectively. At the input (region 0) and output (region N), the expressions change to

$$F_k^0-B_k^0=2\delta_{kM}-\sum_b W_{kb}^{I,1}c_b^1 \tag{18}$$

$$F_k^N-B_k^N=\sum_b W_{kb}^{II,N}c_b^N-2\delta_{kL} \tag{19}$$

where M and L denote the mode of excitation at the input and output, respectively.

Matching the magnetic field components at all discontinuities i leads to matrix equations of the form

$$\left[\nabla T_{hq}^{i-1}\quad \nabla T_{ep}^{i-1}\times\grave{e}_z\right]\begin{bmatrix}Y_{hq}^{i-1}&0\\0&Y_{ep}^{i-1}\end{bmatrix}\begin{bmatrix}F_{hq}^{i-1}-B_{hq}^{i-1}\\F_{ep}^{i-1}-B_{ep}^{i-1}\end{bmatrix}=$$

$$=\left[\nabla T_{hq}^{i}\quad \nabla T_{ep}^{i}\times\grave{e}_z\right]\begin{bmatrix}Y_{hq}^{i}&0\\0&Y_{ep}^{i}\end{bmatrix}\begin{bmatrix}F_{hq}^{i}-B_{hq}^{i}\\F_{ep}^{i}-B_{ep}^{i}\end{bmatrix} \tag{20}$$

By substituting (16) - (19) into (20), multiplying with the components of the vector basis functions (8) and integrating over the aperture area, a set of coupled integral equations is obtained. This procedure is commonly referred to as the method of moments, e.g. [11], in which the testing functions are chosen such that, after integration, the transposed of the coupling matrices [$\underline{W}$] appear. Finally, each equation can be written as

$$[\underline{A}^{i,i-1}]\underline{c}^{i-1}+[\underline{A}^{i,i}]\underline{c}^{i}+[\underline{A}^{i,i+1}]\underline{c}^{i+1}=\underline{0} \tag{21}$$

where

$$[\underline{A}^{i,i-1}]=-[\underline{W}^{I,i}]^T\mathrm{Diag}\{D_s^{i-1}\}[\underline{W}^{II,i-1}] \tag{22}$$

$$[\underline{A}^{i,i}]=[\underline{W}^{I,i}]^T\mathrm{Diag}\{D_t^{i-1}\}[\underline{W}^{I,i}]+[\underline{W}^{II,i}]^T\mathrm{Diag}\{D_t^{i}\}[\underline{W}^{II,i}] \tag{23}$$

$$[\underline{A}^{i,i+1}]=-[\underline{W}^{II,i}]^T\mathrm{Diag}\{D_s^{i}\}[\underline{W}^{I,1+i}] \tag{24}$$

$\underline{c}^i$ are the vectors of expansion coefficients (8) at discontinuity i, T denotes transposed, Diag{} is a diagonal matrix and

$$\{D_t^i\}_k=\frac{Y_k^i}{\tan\{k_{zk}^i L_i\}}\qquad \{D_s^i\}_k=\frac{Y_k^i}{\sin\{k_{zk}^i L_i\}} \tag{25}$$

Slightly different expressions are obtained at the input (region 0, discontinuity 1)

$$[\underline{A}^{1,1}]\underline{c}^1+[\underline{A}^{1,2}]\underline{c}^2=\underline{U} \tag{26}$$

where

$$[\underline{A}^{1,1}]=j[\underline{W}^{I,1}]^T\mathrm{Diag}\{Y^0\}[\underline{W}^{I,1}]+[\underline{W}^{II,1}]^T\mathrm{Diag}\{D_t^1\}[\underline{W}^{II,1}] \tag{27}$$

$$[\underline{A}^{1,2}]=-[\underline{W}^{II,1}]^T\mathrm{Diag}\{D_s^1\}[\underline{W}^{I,2}] \tag{28}$$

$$\underline{U}=j2[\underline{W}^{I,1}]^T\mathrm{Diag}\{Y^0\} \tag{29}$$

and at the output (region N, discontinuity N)

$$[\underline{A}^{N,N-1}]\underline{c}^{N-1}+[\underline{A}^{N,N}]\underline{c}^{N}=\underline{V} \tag{30}$$

where

$$[\underline{A}^{N,N-1}]=-[\underline{W}^{I,N}]^T\mathrm{Diag}\{D_s^{N-1}\}[\underline{W}^{II,N-1}] \tag{31}$$

$$[\underline{A}^{N,N}]=j[\underline{W}^{II,N}]^T\mathrm{Diag}\{Y^N\}[\underline{W}^{II,N}]+[\underline{W}^{I,N}]^T\mathrm{Diag}\{D_t^{N-1}\}[\underline{W}^{I,N}] \tag{32}$$

$$\underline{V}=j2[\underline{W}^{II,N}]^T\mathrm{Diag}\{Y^N\} \tag{33}$$

The final matrix equation, e.g. for six cascaded discontinuities, is given by

$$\begin{bmatrix} \underline{A}^{11} & \underline{A}^{12} & \underline{0} & \underline{0} & \underline{0} & \underline{0} \\ \underline{A}^{21} & \underline{A}^{22} & \underline{A}^{23} & \underline{0} & \underline{0} & \underline{0} \\ \underline{0} & \underline{A}^{32} & \underline{A}^{33} & \underline{A}^{34} & \underline{0} & \underline{0} \\ \underline{0} & \underline{0} & \underline{A}^{43} & \underline{A}^{44} & \underline{A}^{45} & \underline{0} \\ \underline{0} & \underline{0} & \underline{0} & \underline{A}^{54} & \underline{A}^{55} & \underline{A}^{56} \\ \underline{0} & \underline{0} & \underline{0} & \underline{0} & \underline{A}^{65} & \underline{A}^{66} \end{bmatrix} \begin{bmatrix} \underline{c}^1 \\ \underline{c}^2 \\ \underline{c}^3 \\ \underline{c}^4 \\ \underline{c}^5 \\ \underline{c}^6 \end{bmatrix} = \begin{bmatrix} \underline{U} \\ \underline{0} \\ \underline{0} \\ \underline{0} \\ \underline{0} \\ \underline{V} \end{bmatrix} \tag{34}$$

and exhibits the following properties:

1. The size of matrix [A] is N times the number of basis functions, and the number of basis functions per discontinuity need not be constant.
2. The modes enter matrix elements through sums (matrix multiplications) which can individually be checked for convergence. Note that this procedure eliminates the phenomenon of relative convergence known from mode-matching techniques [2].
3. Matrix [A] is block-diagonal and symmetric. If the structure under investigation is symmetric in the direction of propagation, then [A] is also symmetric with respect to its minor diagonal. Hence only a limited number of matrix entries need to be computed.
4. An LU decomposition (under consideration of the block structure and symmetries) needs to be performed only once per frequency point.
5. For all different excitation vectors U, V, only coefficient vectors $\underline{c}^1$, $\underline{c}^N$ are required to compute the scattering parameters (see below). Moreover, for excitation at the input, $\underline{V}=\underline{0}$ and, for excitation at the output, $\underline{U}=\underline{0}$.
6. The number of modes required in the generalized scattering matrix representation of the component under investigation is usually much smaller than those considered at the individual discontinuities within the component. If the component is symmetric, only one excitation vector is required to obtain the fundamental-mode scattering parameters.

The scheme of (34) is obviously not suited to treat a single discontinuity. In such a case, the equations are rewritten to yield

$$[\underline{A}^{I,I}]\underline{c}^I = \underline{U} + \underline{V} \tag{35}$$

where

$$[\underline{A}^{I,I}] = [\underline{W}^{I,I}]^T \mathrm{Diag}\{Y^0\}[\underline{W}^{I,I}] + [\underline{W}^{II,I}]^T \mathrm{Diag}\{Y^N\}[\underline{W}^{II,I}] \tag{36}$$

$$\underline{U} = 2[\underline{W}^{I,I}]^T \mathrm{Diag}\{Y^0\} \tag{37}$$

$$\underline{V} = 2[\underline{W}^{II,I}]^T \mathrm{Diag}\{Y^I\} \tag{38}$$

and, under consideration of above item 5, either $\underline{V}=\underline{0}$ or $\underline{U}=\underline{0}$.

c) Extraction of the Generalized Scattering Matrix

Let $\underline{c}^I_M$, $\underline{c}^N_M$, $\underline{c}^I_L$, $\underline{c}^N_L$ be the coefficient vectors at the first (1) and last (N) discontinuity due to excitation by the Mth mode at the input and the Lth mode at the output. Then a column vector of the unnormalized generalized scattering matrix is obtained through

$$(\bar{\underline{S}}_{11})_M = [\underline{W}^{I,I}]\underline{c}^I_M - \delta_{kM} \tag{39}$$

$$(\bar{\underline{S}}_{21})_M = [\underline{W}^{II,N}]\underline{c}^N_M \tag{40}$$

$$(\bar{\underline{S}}_{22})_L = [\underline{W}^{II,N}]\underline{c}^N_L - \delta_{kL} \tag{41}$$

$$(\bar{\underline{S}}_{12})_L = [\underline{W}^{I,I}]\underline{c}^I_L \tag{42}$$

Once all column vectors have been computed to form the matrix $[\bar{\underline{S}}]$, the final S-matrix requires a power normalization by the square roots of the frequency-dependent admittances.

$$[\underline{S}_{11}]_{kM} = [\bar{\underline{S}}_{11}]_{kM}\sqrt{Y^0_k/Y^0_M} \tag{43}$$

$$[\underline{S}_{21}]_{kM} = [\bar{\underline{S}}_{21}]_{kM}\sqrt{Y^N_k/Y^0_M} \tag{44}$$

$$[\underline{S}_{22}]_{kL} = [\bar{\underline{S}}_{22}]_{kL}\sqrt{Y^N_k/Y^N_L} \tag{45}$$

$$[\underline{S}_{12}]_{kL} = [\bar{\underline{S}}_{12}]_{kL}\sqrt{Y^0_k/Y^N_L} \tag{46}$$

Note that the frequency-independent components of the power normalization have been incorporated in the potential functions (1), (2).

III. RESULTS

This section shows some results obtained by the theory presented above. Calculations by our own MMT routines, which always use the smallest possible matrix for matrix inversions, are mostly used as reference values. Other comparisons are carried out using a commercial field solver and data from the literature. In order to dem-

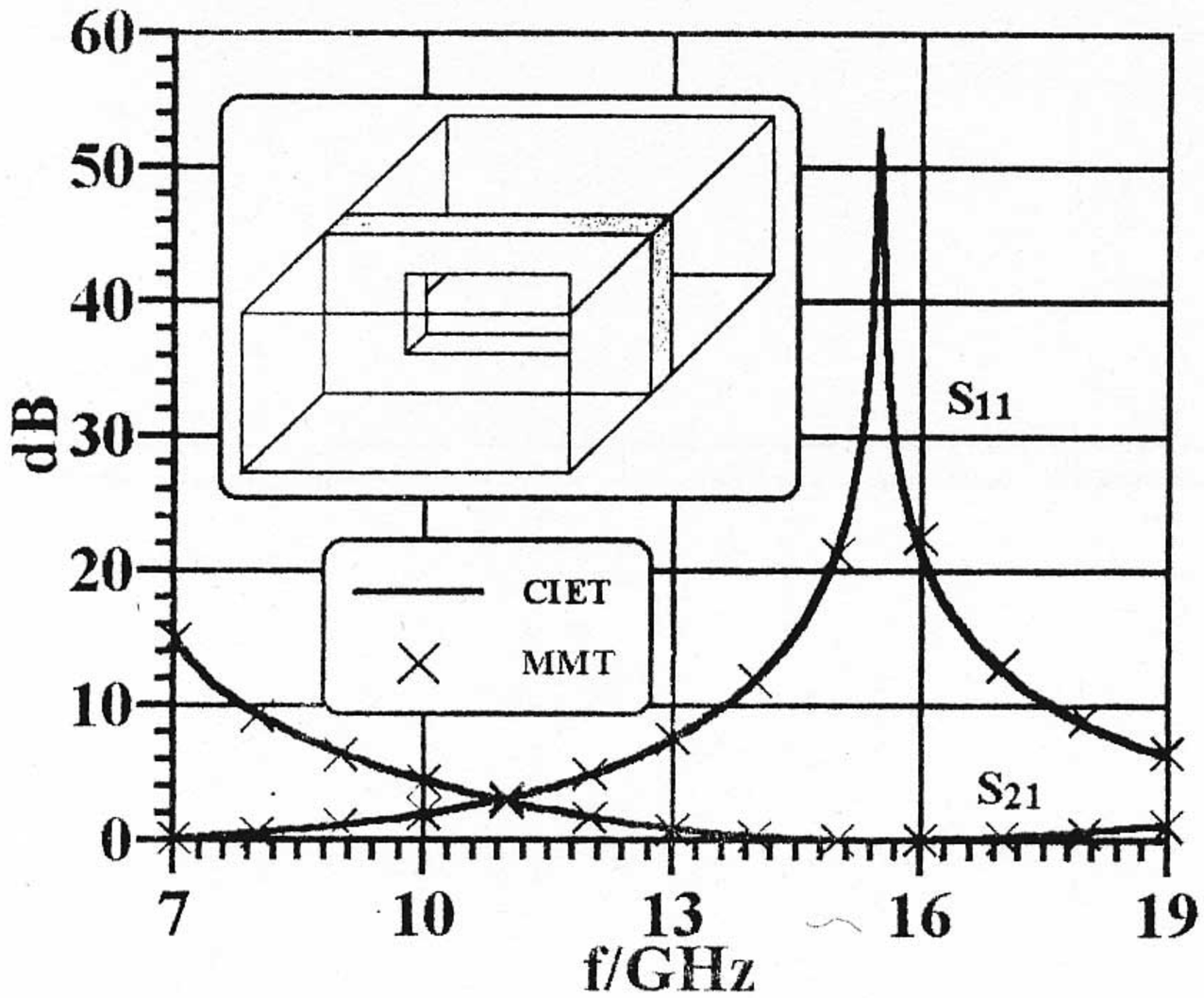

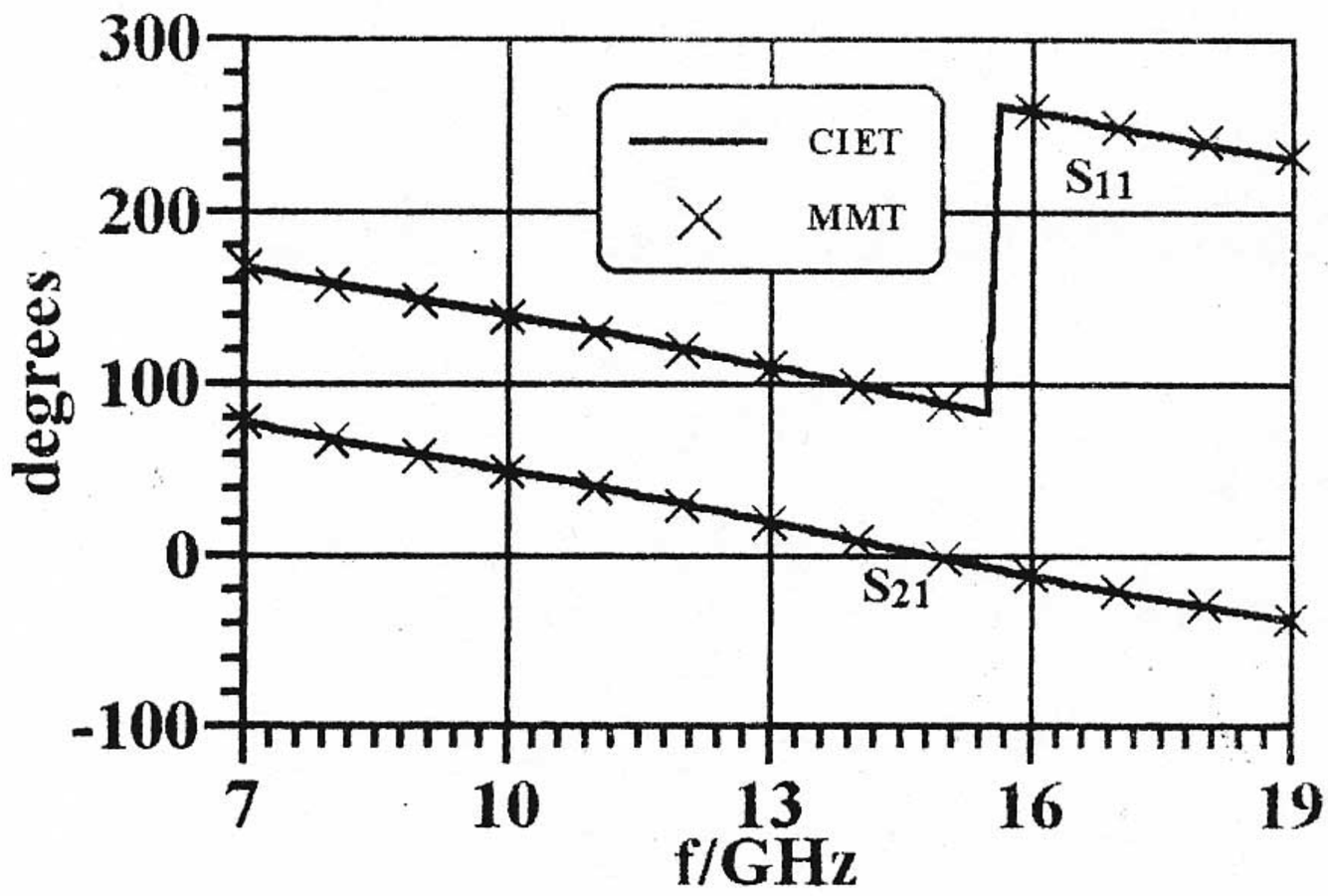

Figure 4: Comparison between CIET (solid lines) and MMT (x) at an iris in X-band waveguide; waveguide dimensions: a=22.86mm, b=10.16mm; iris dimensions: a_0=11.43mm, b_0=5.08mm, L=1.0mm.

onstrate typical performance ranges, some of the components have been designed by linking CIET to a MiniMax-based optimization algorithm [12].

Fig. 4 shows a comparison between CIET and MMT at a simple resonant-iris structure with TE_{10}-mode field symmetry. Excellent agreement is obtained for both magnitude and phase performance. The iris resonance at 15.5 GHz is accurately modelled by both routines.

The waveguide twist component of Fig. 5 [13] is used for verification of rectangular discontinuities of the more general kind. From input to output, the incoming vertical polarization undergoes three 90-degree field rotations. Excellent agreement is obtained between the CIET (solid lines) and the MMT (dashed lines). However, with up to 86 modes in both methods and up to 16 basis functions in the CIET, the CIET is 100 times faster than the MMT. Using 25 modes and 12 basis functions, which gives return loss results within 2.5dB of those shown in Fig. 5, the CIET routine is still ten times faster than that using the MMT.

An 11-stub high-pass E-plane stub filter with matching transformer sections is shown in Fig. 6. X-band performance specifications include 90 dB rejection between 8 GHz and 10.2 GHz and 33 dB return loss in the 10.7 - 13.0 GHz band. The CIET analysis is performed using 48 TE_{1n} and 47 TM_{1n} modes and three TE_{1n}- and two TM_{1n}-mode basis function. Even though

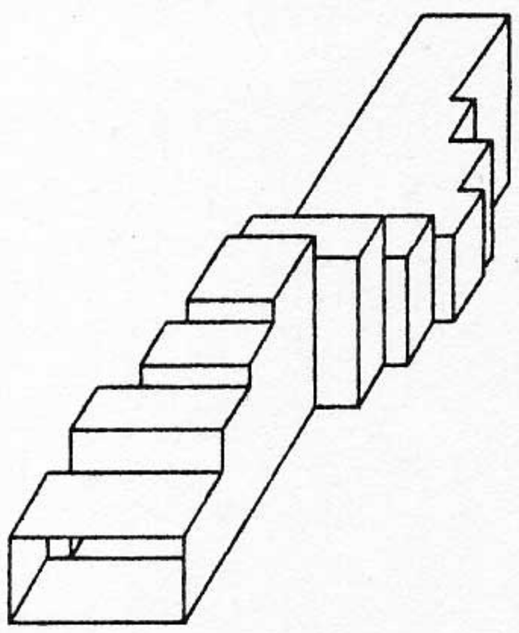

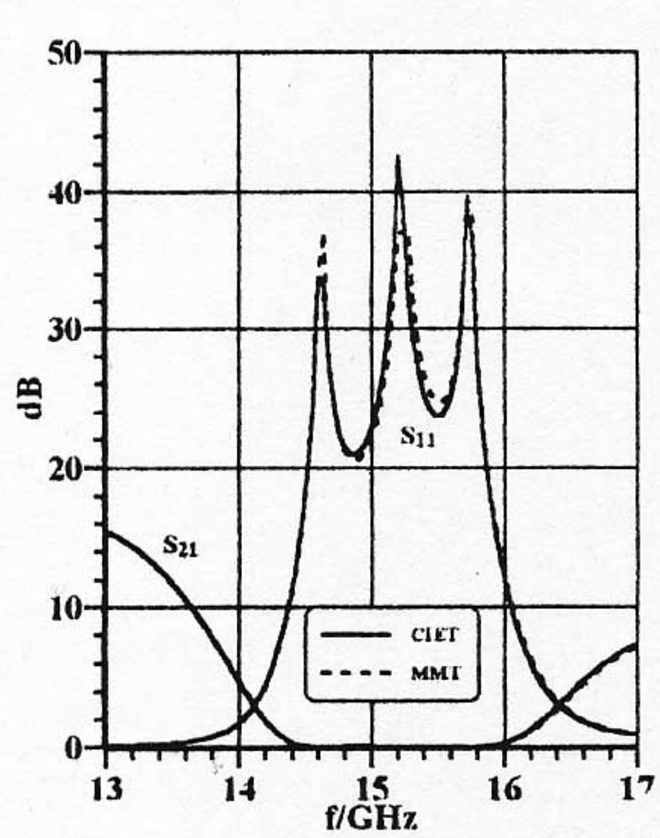

Figure 5: Comparison between CIET (solid lines) and MMT (dashed lines) at an integrated waveguide 270-degree twist component according to [13].

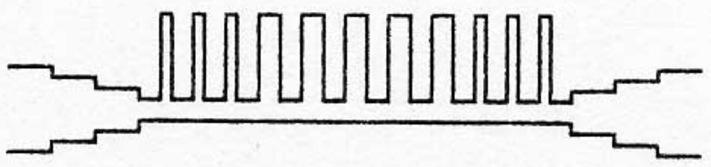

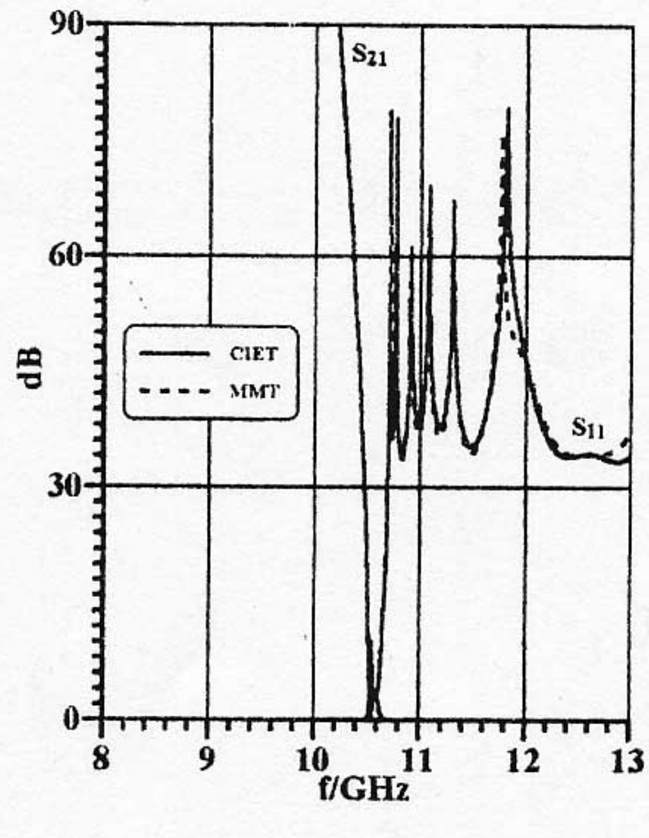

Figure 6: Performance of a 11-stub E-plane high-pass filter with two-section waveguide transformers for connection to standard X-band waveguide; CIET (solid lines), MMT (dashed lines).

the MMT is formulated with longitudinal TE_{1n}-to-x modes, the CIET routine is still 4.5 times faster than MMT. If also the CIET is formulated with TE_{1n}-to-x modes, then this factor increases to approximately 35 [14].

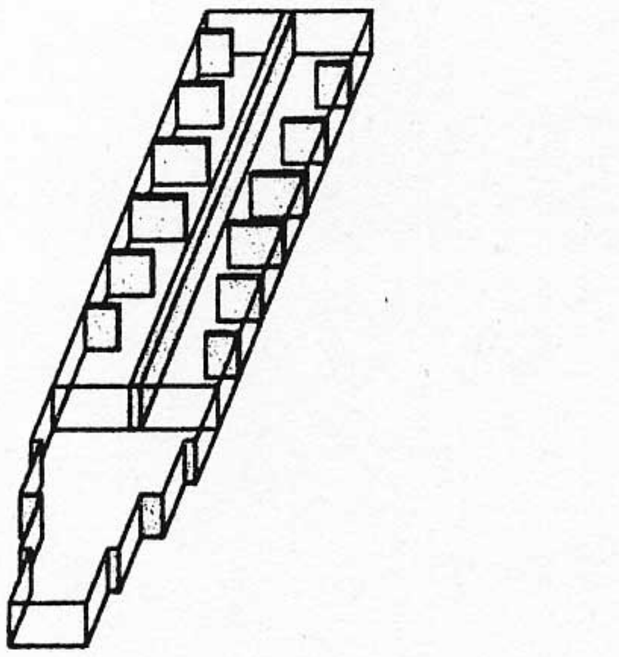

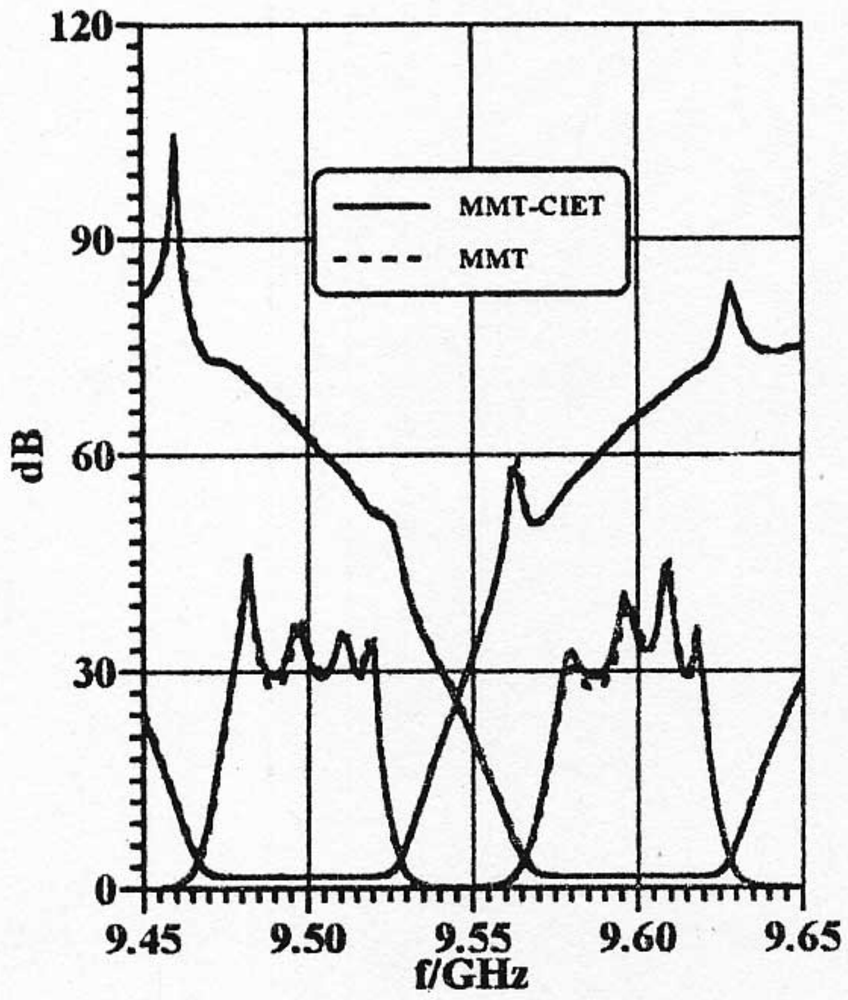

Figure 7. Narrowband H-plane bifurcation diplexer utilizing five-resonator single-sided inductive-iris filters; filter analysis by CIET and power divider by MMT (solid lines), all-MMT (dashed lines).

An example for the ability of CIET to extract the generalized scattering matrix is shown in Fig. 7. Both narrowband filters in the H-plane diplexer arrangement are analyzed by the CIET using 100 TE_{m0} modes and seven basis functions. The matching input transformer and the H-plane bifurcation are computed by the MMT. Both methods are interfaced with the respective generalized S-matrices retaining 15 TE_{m0} modes. Excellent agreement is obtained between the combination of CIET and MMT (solid lines) and an all-MMT computation (dashed lines). Both calculations include a loss analysis

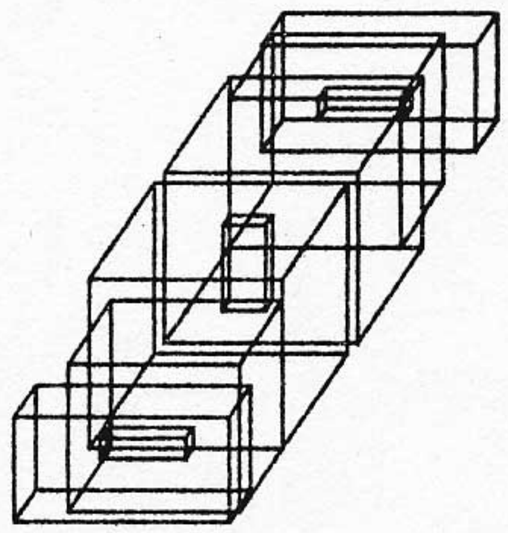

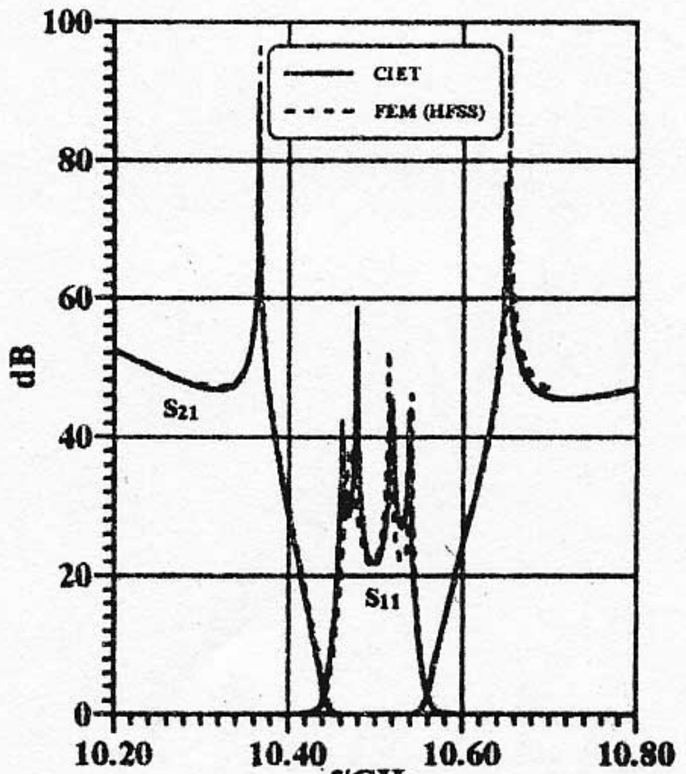

Figure 8: Performance of a four-pole inline dual-mode filter for X-band applications; this method (solid lines), finite-element method (HFSS, dashed lines).

based on the TE_{10}-mode resonances, the loaded Q value of the cavities and the bandwidths of the channel filters [15]. In several different designs of such diplexers for terrestrial communication systems, the algorithm using the CIET has been demonstrated to be at least 25 times as fast as the all-MMT routine.

The four-pole dual-mode filter structure shown in Fig. 8 was one of the main motivations for the development of the CIET. Owing to the inline configuration and the two field polarizations involved, the complete set of TE_{mn}-TM_{mn} modes must be considered in the analysis. With the MMT, although up to 415 modes were used, an initial design could not be brought into a range of convergence within a reasonable time frame. The filter was then analyzed and optimized by the CIET with up to 1740 modes and up to 23 basis functions. The final analysis was performed with up to 3900 modes and is shown as solid lines in Fig. 8. A comparison with Hewlett Packard's finite-element package HFSS (dashed lines) shows very good agreement. HFSS went through 40 mesh refinement steps until convergence was reached within our maximum allocated memory of 800 MB.

As mentioned earlier, the general theory of cascading discontinuities in CIET is not restricted to the cartesian coordinate system. Fig. 9 shows a three-resonator circular waveguide TE_{11}-mode iris filter, which has been used in an initial feed design to improve the isolation of a feed chain towards a lower frequency band. The CIET uses edge-conditioned vector basis functions in the circular-cylindrical coordinate system [16]. The agreement with an MMT-based routine is extremely good. The CIET algorithm is only one order of magnitude faster than that using the MMT. This is largely attributed to the fact that in the circular-cylindrical sys-

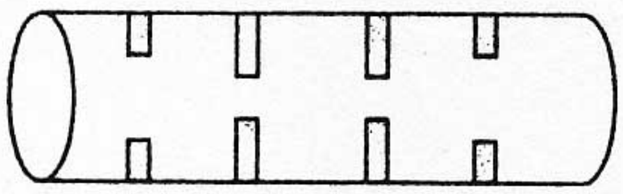

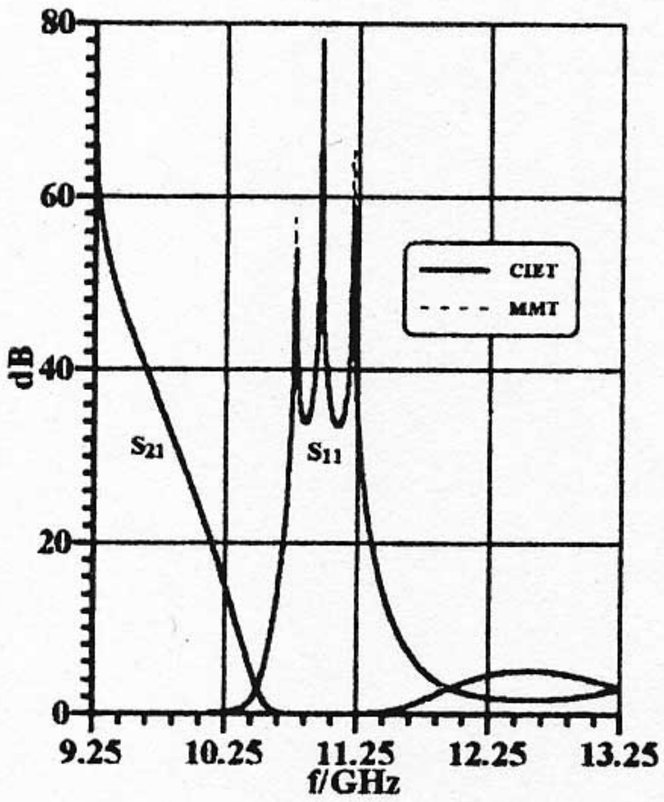

Figure 9: Performance of three-resonator circular waveguide TE_{11}-mode filter for X-band applications; CIET (solid lines), MMT (dashed lines).

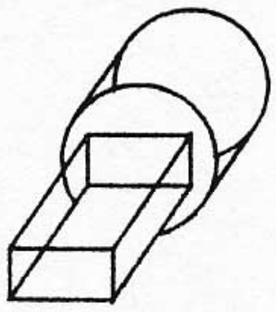

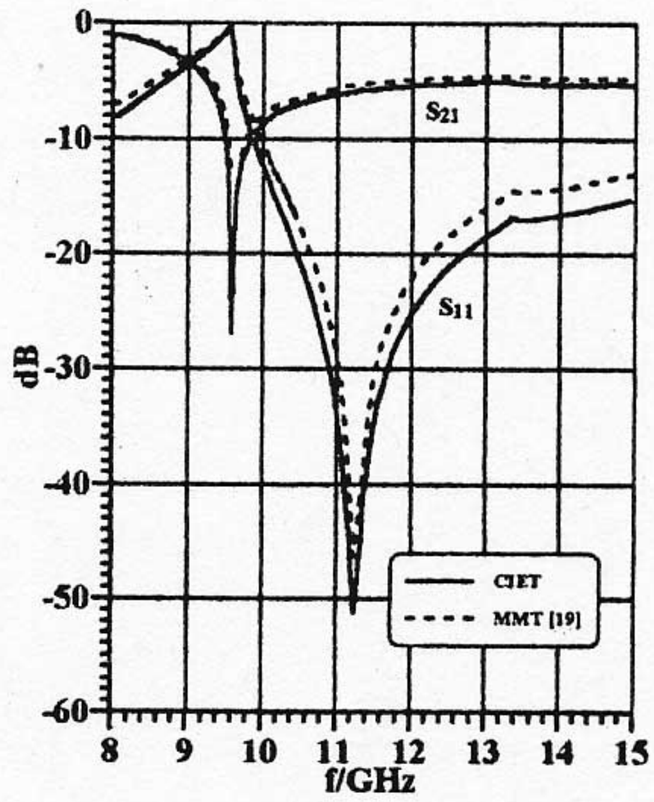

Figure 10: Rectangular-to-circular waveguide transition according to [19]; CIET (solid lines), MMT (dashed lines) [19].

tem, the entries of the coupling matrices [W] need to be evaluated numerically whereas, in the MMT, analytic solutions are available, e.g., [17].

As an example of a structure involving a mixed coordinate system, Fig. 10 shows results for a rectangular-to-circular waveguide transition [18], [19]. Whereas the resonances are excellently modelled by both the CIET and the MMT [18], some discrepancies, the causes of which are yet to be determined, are observed in the return-loss behaviour towards higher frequencies.

IV. CONCLUSIONS

The coupled-integral-equations technique is a fast, powerful and effective tool for the analysis of waveguide discontinuities. Its most attractive features are the simultaneous inclusion of edge conditions at all discontinuities, the highly sparse system matrix and the nonexistence of the relative convergence phenomenon known from mode-matching techniques. The CIET is especially effective in narrowband systems where both the MMT and many commercial field solvers have extremely high demands for computing resourses.

Acknowledgement: The authors would like to thank Uwe Rosenberg of Bosch Telecom, Backnang, Germany for the initial design of the dual-mode filter displayed in Fig. 8.

REFERENCES

[1] J. Uher, J. Bornemann and U. Rosenberg, Waveguide Components for Antenna Feed Systems. Theory and CAD, Artech House, Norwood 1993.

[2] T. Itoh ed., Numerical Techniques for Microwave and Millimeter-Wave Passive Structures, John Wiley & Sons, New York 1989.

[3] B. Veidt, Microwave J., Vol. 41, pp. 126-137, Sep. 1998.

[4] R. Beyer and F. Arndt, 1998 IEEE MTT-S Int. Microwave Symp. Dig., pp. 1275-1278, Baltimore, USA, June 1998.

[5] R. Sorrentino, M. Mongiardo, F. Alessandri and G. Schiavon, Int. J. Numerical Modelling, Vol. 4, pp. 19-43, March 1991.

[6] T. Rozzi and M. Mongiardo, IEEE Trans. Microwave Theory Tech., Vol. 30, pp. 1279-1288, Aug. 1991.

[7] S. Amari, J. Bornemann and R. Vahldieck, IEEE Trans. Microwave Theory Tech., Vol. 45, pp. 1611-1618, Sep. 1997.

[8] R. E. Collin, Field Theory of Guided Waves, IEEE Press, New York, 1991.

[9] I. S. Gradshteyn and I. M. Ryznik, Tables of Integrals, Series, and Products, Fifth Edition, Academic Press, New York, 1994.

[10] W.H. Press, B.P.Flannery, S.A. Teukolsky and W.T. Vetterling, Numerical Recipes. The Art of Scientific Computing, 2nd ed., Cambridge University Press, Cambridge 1995.

[11] R. F. Harrington, Field Computation by Moment Methods, Krieger, Malabar, Fl. 1987.

[12] K. Madsen, H. Schaer-Jacobsen and J. Voldby, IEEE Trans. Circuits Systems, Vol. CAS-22, pp. 791-796, Oct. 1975.

[13] J. Bornemann, IEE Proc.-Microw. Antennas Propag., Vol. 142, pp. 345-349, Aug. 1995.

[14] S. Amari, J. Bornemann and R. Vahldieck, J. Electro. Waves Applic., Vol 13, 1999 (in press).

[15] G. Matthaei, L. Young and E.M.T. Jones, Microwave Filters, Impedance-Matching Networks, and Coupling Structures, Dedham: Artech House, 1980.

[16] S. Amari, R. Vahldieck and J. Bornemann, 1998 IEEE AP-S Int. Symp. Dig., Atlanta, USA, pp. 268-271, June 1998.

[17] H.D. Knetsch, Arch. Elektr. Übertr., Vol. 23, pp. 23-32, Jan. 1969.

[18] T. Lenadan, S. Amari, R. Vahldieck and J. Bornemann, 1997 IEEE MTT-S Int. Microwave Symp. Dig. , pp. 207-210, Denver, USA, June 1997.

[19] R.H. MacPhie and K.-L. Wu, IEEE Trans. Microwave Theory Tech., Vol. 43, pp. 2041-2045, Sep. 1995.